Valence State Tuning of Gold Nanoparticles in the Dewetting Process: An X-ray Photoelectron Spectroscopy Study

Gustavo Lanza, Mawin J. Martinez Jimenez, Fernando Alvarez, Jaime Andres Perez-Taborda, and Alba Avila*
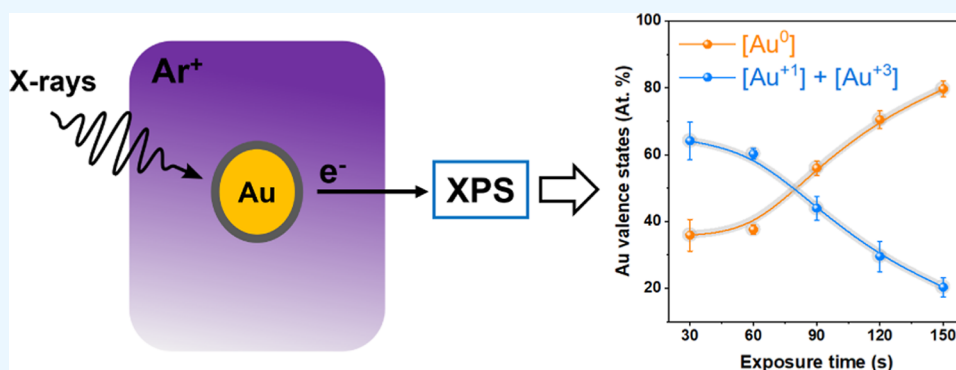
ACCESS | Metrics & More | Article Recommendations | Supporting Information

ABSTRACT: Gold nanoparticles (AuNPs) are commonly synthesized using the citrate reduction method, reducing Au^{3+} into Au^{1+} ions and facilitating the disproportionation of aurous species to Au atoms (Au^0). This method results on citrate-capped AuNPs with valence single states Au^0. Here, we report a methodology that allows obtaining AuNPs by the dewetting process with three different valence states (Au^{3+}, Au^{1+}, and Au^0), which can be fine-tuned with ion bombardment. The chemical surface changes and binding state of the NPs were investigated using core-level X-ray photoelectron spectroscopy (XPS). This is achieved by recording high-resolution Au 4f XPS spectra as a function of ion dose exposure. The results obtained show a time-dependent tuning effect on the Au valence states using low-energy 200 V acceleration voltage Ar^+ ion bombardment, and the valence state conversion kinetics involves the reduction from Au^{3+} and Au^{1+} to Au^0. Proper control of the reduction in the valence states is critical in surface engineering for controlling catalytic reactions.

INTRODUCTION

Gold nanoparticles (AuNPs) have attracted great interest in sensing systems due to their exceptional optical, electronic, and chemical properties.[1−3] Particularly, AuNPs with specific morphologies such as nanospheres, nanostars, nanorods, nanotriangles, and nanopolyhedrons have been widely integrated into biosensors and surface-enhanced Raman scattering applications. The properties of these kinds of AuNPs are explained through localized surface plasmon resonance (LSPR), as described by Mie's theory.[4] LSPR is a phenomenon related to the collective oscillation of AuNP free electrons interacting with a specific electromagnetic wave in the visible range. This phenomenon is strongly dependent on the shape, size, and surrounding medium of the AuNPs.[5,6] Conventionally, AuNPs are successfully obtained by chemical routes, but byproducts are generated with a harmful impact on human health and the environment.[7] Therefore, solid-state dewetting of gold thin films emerges as an alternative for the large-scale production of functional plasmonic nanostructures.[8] Dewetting is a spontaneous phenomenon, in which a thin film

on a suitable substrate is broken down into small particles, a process mediated by the minimization of surface energy.[9]

In recent studies, compositional analysis studies of AuNPs and their valence states show other interesting properties for potential applications in chemical technology, such as catalysis.[10,11] AuNPs with Au^{1+} and Au^{3+} valence states have been shown to be the most active catalyst for carbon monoxide oxidation at room (or lowest) temperature, electrochemical nitrogen reduction reaction to ammonia (NH_3), and liquid phase oxidation of alcohols. Casaletto et al.[12] showed that the presence of the Au^{1+} species seems to be the main requirement for obtaining the highest CO conversion at the lowest temperature due to better stabilization of the AuO^- species.
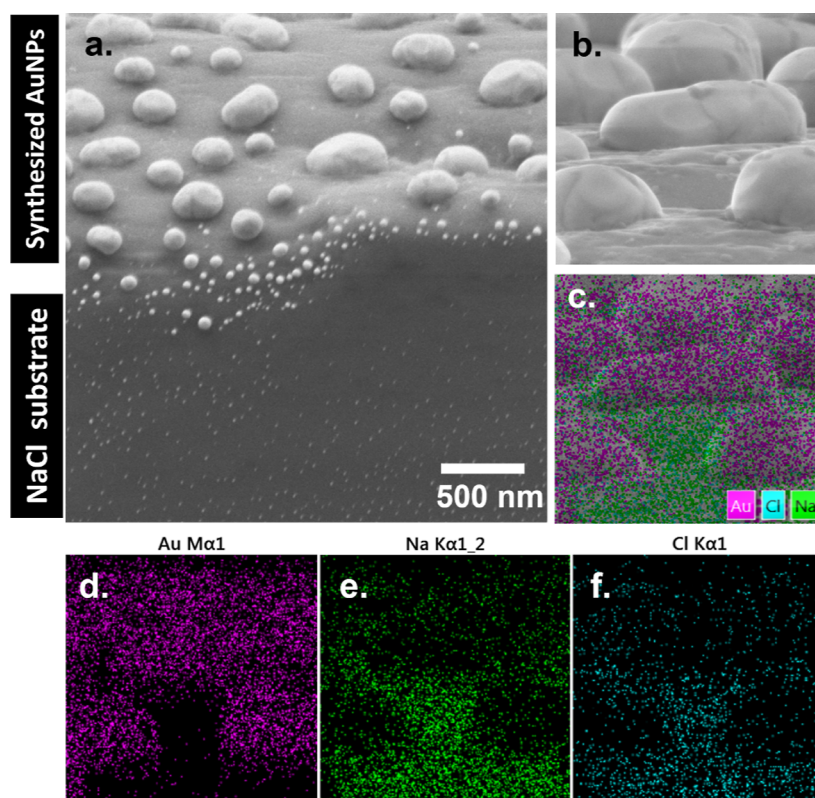
Figure 1. AuNPs synthesized on a NaCl substrate by the dewetting process: (a) cross-section image of the NaCl substrate and AuNPs synthesized; (b)AuNPs synthesized; (c) compositional mapping of the AuNPs [image (b)]; and (d−f) mapping of Au, Na, and Cl, respectively, of the AuNPs (image b).

Zheng et al.[13] reported that the presence of the Au^{1+} oxidation state increases the effectiveness of the (photo)electrochemical N_2 reduction reaction and proposed that adjusting the Au oxidation state could increase the reduction efficiency and selectivity from N_2 to NH_3. Pakrieva et al.[14] investigated the role of the various electronic oxidation states of Au on the catalytic behavior of the liquid phase oxidation of *n*-octanol. They showed that Au^{3+} inhibited the oxidation process, while Au^{1+} was the active site state, and Au^0 had a negative effect due to the partial blocking of Au^0 by the solvent. As it can be seen, the size and shape of AuNPs define their physical properties, and the valence state plays an important role in the catalytic activity of AuNPs. Using experimental physical methods, tuning AuNP valence states has been taken in consideration. Ion bombardment is a promising technique allowing tailoring oxidation states in process setting for the proposed challenge by a fine control of both bombarding acceleration voltage and ion dose.[15,16]

Ion bombardment of solids is a well-established methodology for etching, modifying the surface, or causing structural defects at the nanometer scale.[17] For example, during bombardment with Ar^+ ions on thin films of TiO_2, oxygen atoms are preferentially ejected, causing chemical reduction to lower Ti valence states (even for metal) and can induce its transformation into a single-crystalline TiO.[18,19] Likewise, Ar^+ ion bombardment has been shown to modify the chemical states of W in WO_3 nanowires. Intermediate oxidation states were reported in the reduction process of WO_3 to metallic W.[20] Several experimental approaches have been carried out on the effect caused by ion beam irradiation on AuNPs on top of various substrates. The thermodynamic driving force resulting from the interaction between the AuNPs and the substrate when it is under Ar^+/Xe^+ ion bombardment produces effects such as burrowing and dewetting, which are explained by the minimization of the surface free energy.[21,22] Although the burrowing on AuNPs has been studied, the effects produced by Ar^{1+} ion bombardment on the changes in the valence states of AuNPs are still scarce. This contribution investigates the controlled modification in the valence states, which will allow expanding the previously reported approaches and increasing the possible number of technological applications of AuNPs.

Here, AuNPs were obtained by using solid-state dewetting of an Au thin film. The chemical state of Au in AuNPs has been examined in detail as a function of accumulated Ar^+ dose by using core-level X-ray photoelectron spectroscopy (XPS). We demonstrate that different Au oxidation valence states can be obtained by precise Ar^+ bombardment of the AuNPs, owing to the ion-induced reduction effect.

■ RESULTS AND DISCUSSION

Morphology and Optical Properties of AuNPs. AuNPs were physically synthesized by solid-state thermal dewetting of thin gold films, in accordance with the Patent NC2021/000297[23] (see details in the Experimental Section). The scanning electron microscopy (SEM) micrographs in Figure 1a,b shows the typical structure of the as-prepared AuNPs onto the NaCl substrate, which consists of nanometric particles of various sizes and shapes.

Energy dispersion spectroscopy (EDS) elemental maps were recorded in several top-surface regions of the substrate and AuNPs, as presented in Figure 1c,d−f, respectively. Traces of Na and Cl are evident in the AuNPs synthesized. The AuNPs
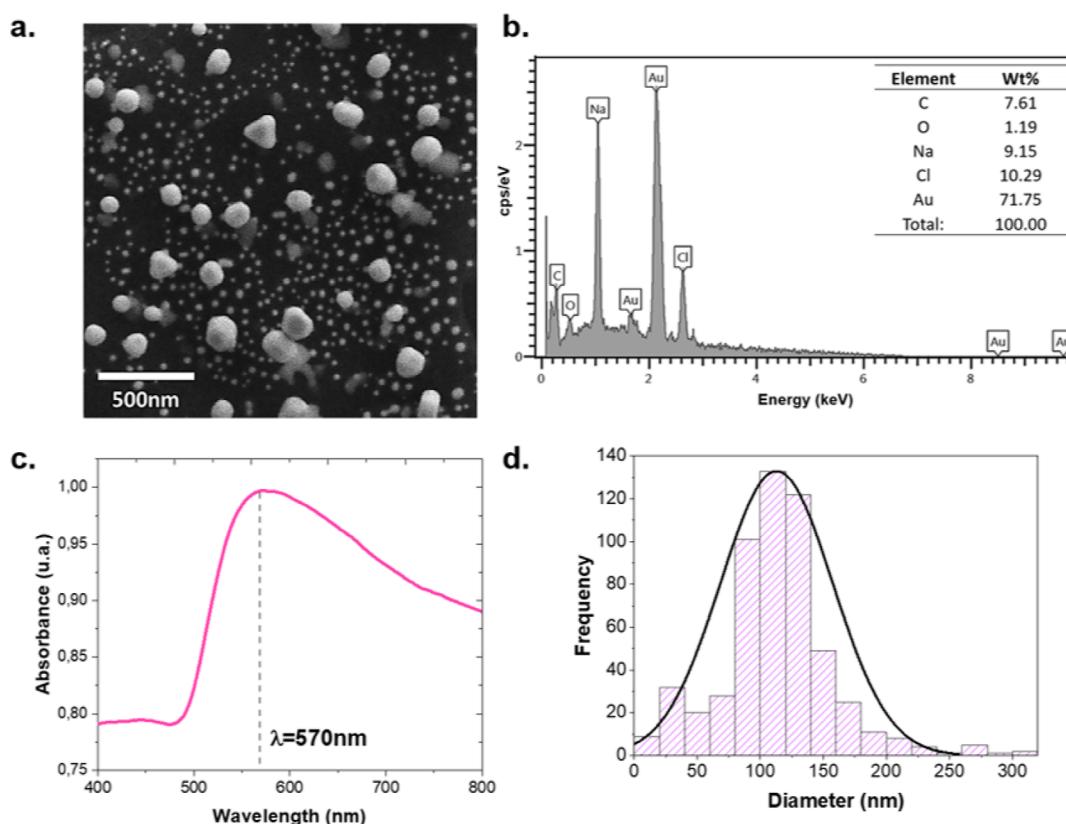
Figure 2. Morphological, compositional, and optical characterization of AuNPs in the suspension obtained from a dewetting process: (a) SEM image; (b) EDS spectra; (c) UV−vis absorption spectra; and (d) size distribution.

were collected by dripping water on the substrate, resulting in homogeneous, stable AuNP water suspension with pH = 6.45 ± 0.5. Initially, characterization of the synthesized AuNPs without treatment of Ar^+ bombardment was carried out. Figure 2a shows a typical sample's SEM image of AuNPs after collection. From the SEM image, it can be seen that the synthesized nanoparticles are not in a preferential shape (polyphormic), and AuNPs in the range from ∼70 to ∼170 nm with a polydispersity index of 0.36 were obtained.

The EDS characterization (Figure 2b) shows nanoparticles with a majority composition of Au (71.75 ± 0.88 wt %) and the presence of a lower percentage of Na (9.15 ± 0.33 wt %) and Cl (10.29 ± 0.50 wt %). The above suggests the remanence of Na and Cl atoms in the nanoparticles due to the drag of these elements during the dewetting process. This is due to the stress prompted in the thin Au films during annealing, causing the film to break, leading to the nanoparticles final synthesis (see Figure 1). Figure 2c reports the experimental absorption spectra in the wavelength range between 400 and 800 nm of AuNPs in the suspension. The absorption spectrum of AuNPs suspended shows a strong absorption band with a maximum at 570 nm due to LSPR.[24] The use of NaCl in the synthesis process generates a new absorbance band at a longer wavelength, as reported by Zimbone et al.[25]

XPS Characterization: Chemical Surface Changes. The results obtained by the EDS characterization were corroborated by X-ray photoelectron spectroscopy (XPS), where the presence of Au, Na, and Cl was also observed. However, we will focus on the use of XPS characterization to elucidate the effects of Ar^+ ion bombardment in a high vacuum

chamber, owing a Kaufman ion gun attached to a hight vacuum chamber for XPS analysis to study the reduction kinetics of Au valence states. Details of the system can be consulted in ref 26. The ion bombardment-induced changes were analyzed by using a Thermo Alpha 110 Hemispherical Analyzer. The XPS spectra were recorded using the 1486.6 eV photons from an Al target ($K\alpha$ line), in the constant energy pass mode (CPM, 40 eV). CasaXPS software carried out the XPS peak fitting, and the Shirley method removed the electron inelastic collision background. Each Ar^+ ion bombardment step was performed with 200 V acceleration voltage under ∼2 × 10^{-2} Pa Ar pressure for 30 s. A sputtering rate of 0.53 nm/s was calculated from the difference in the average diameters of the AuNPs by the exposure time before and after the 150 s Ar^+ ion bombardment.

Figure 3 displays the high-resolution spectra of the region corresponding to the Au 4f core levels observed for AuNPs, recorded after stepwise Ar^+ sputtering processes. In the initial stage, the separation between the two typical peaks formed by the Au $4f_{7/2}$ and Au $4f_{5/2}$ spin−orbital splitting photoelectrons of AuNPs is not well defined (see Figure 3a,b), which is associated with the presence of different valence states of Au (Au^{3+}, Au^{1+}, and Au^0),[27] being Au^1 the majority state. However, peak separation is well defined after the third stage of irradiation with Ar^+ ions (Figure 3c,d,f), with a substantial increase in the Au^0 valence state while Au^{1+} and Au^{3+} decrease.

The aforementioned is more explicit in Figure 4a, where the concentration of Au^0 valence states and the sum $[Au^{1+}]$ + $[Au^{3+}]$ are plotted as a function of accumulated exposure time with 200 V acceleration voltage. The ratio between $[Au^0]$ and $[Au^{1+}]$ + $[Au^{3+}]$ as a function of accumulated exposure time is
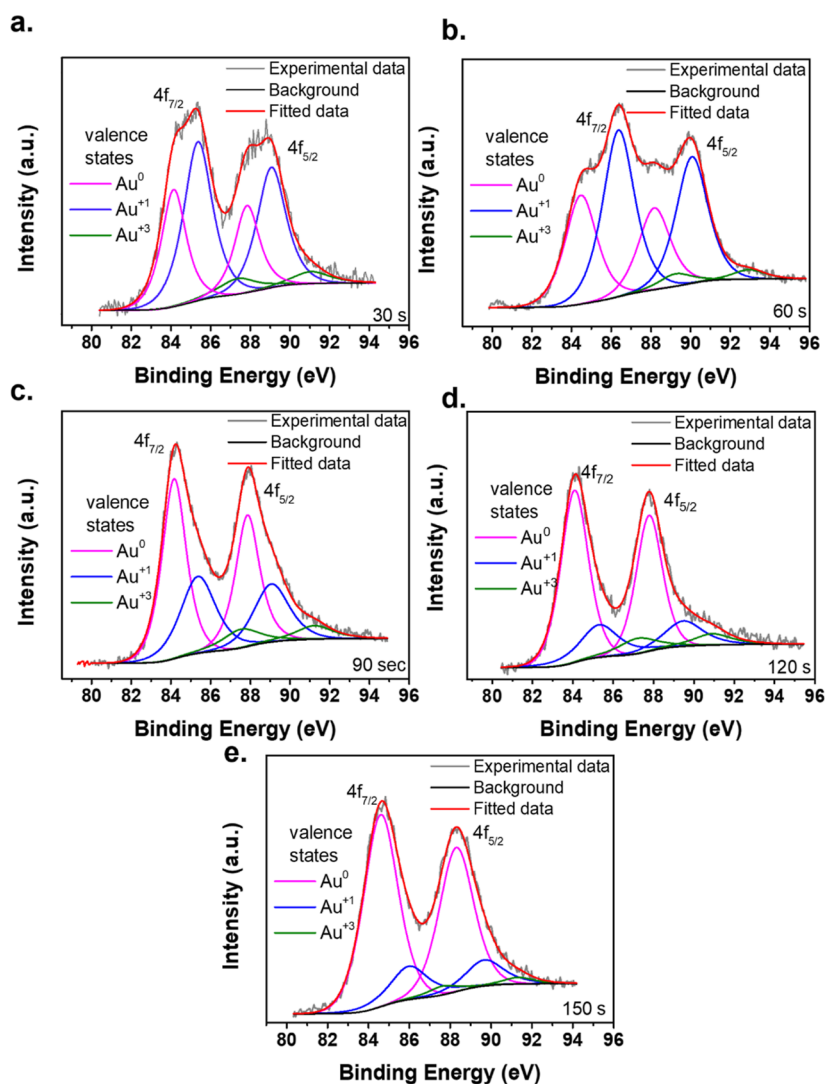
Figure 3. High-resolution Au 4f XPS spectra obtained after each step of Ar$^+$ bombardment with 200 V acceleration voltage on AuNPs for 30 s. The time shown is cumulative time to exposure: (a) 30 s; (b) 60 s; (c) 90 s; (d) 120 s; and (e) 150 s.
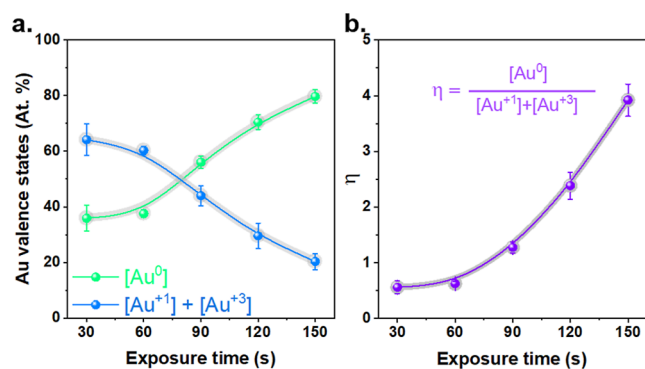

Figure 4. Evolution of valence state concentration: (a) [Au^0] and [Au^{1+}] + [Au^{3+}] as a function of accumulated time of exposure to Ar$^+$ ion bombardment; (b) ratio between [Au^0] and [Au^{1+}] + [Au^{3+}] as a function of accumulated exposure time.

shown in Figure 4b, showing an exponential increase after each exposure step during Ar$^+$ bombardment on the AuNP surface. That is, the oxidation states of AuNPs were changed to lower oxidation states of Au due to preferential sputtering of O, Na, and Cl on the AuNP surface by Ar$^+$ bombardment, commonly

observed in metal compounds.[28] SEM image and compositional analysis by EDS after 150 s of Ar$^+$ ion bombardment is shown in Figure S1.

On the other hand, the high-resolution XPS spectra of the Cl 2p can be deconvoluted by assuming contribution from the Cl−Au, −C$_x$Cl, and Cl−O chemical species.[29,30] Each chemical state has associated two peaks that correspond to Cl 2p$_{1/2}$ and Cl 2p$_{3/2}$ spin−orbital splitting photoelectrons (∼1.6 eV), as can be seen in Figure 5 (the Cl 2p spectra are normalized, see Figure S2). XPS spectroscopy clearly demonstrates that Cl and O not only cover the surface but are also within AuNPs, while Na disappears after the second Ar$^+$ ion bombardment (Figure S3). The reduction of Au^{3+} to lower valence states is due to the desorption of oxygen and chlorine radicals, leading to the production of oxygen and chlorine gas during exposure to ion bombardment; this is observed in the changes in the shape of the O 1s and Cl 2p core-level spectra.

The valence state conversion kinetics of Au follows the model proposed by Fong et al.[31] This involves the reduction kinetics from Au^{3+} and Au^{1+} to Au^0 according to
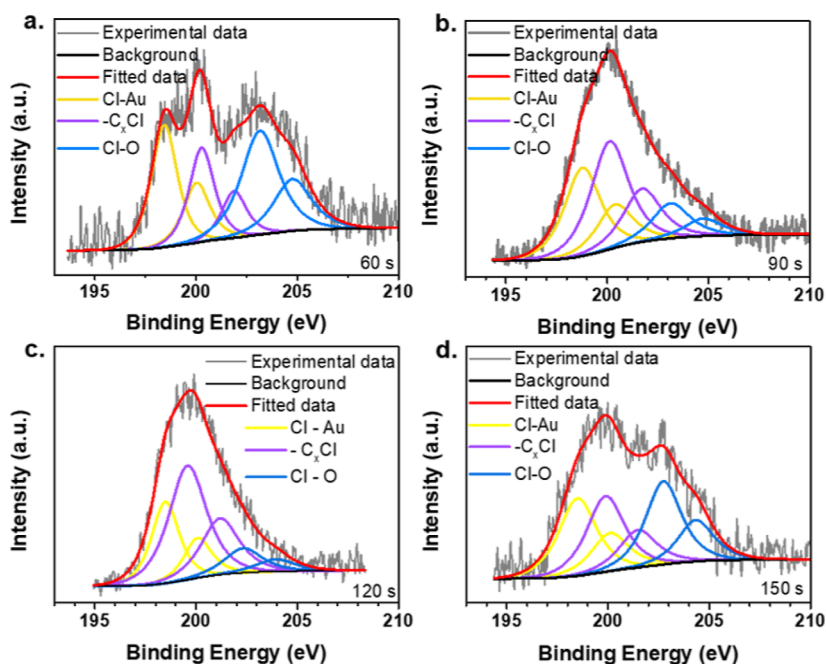
Figure 5. Representative fitted Cl 2p core-level spectra acquired after (a) 60 s, (b) 90 s, (c) 120 s, and (d) 150 s of accumulated exposition time with 200 V acceleration voltage Ar$^+$ ion bombardment.

$$\frac{d}{dt}\text{Au}^{3+} = k_{-1}[\text{Au}^{1+}] - k_1[\text{Au}^{3+}]$$

$$\frac{d}{dt}\text{Au}^{1+} = k_1[\text{Au}^{3+}] - k_{-1}[\text{Au}^{1+}] - k_2[\text{Au}^{1+}] + k_{-2}[\text{Au}^0]$$

$$\frac{d}{dt}\text{Au}^0 = k_2[\text{Au}^{1+}] - k_{-2}[\text{Au}^0]$$

where k_1, k_{-1}, k_2, and k_{-2} are the rate constants for the reduction. Au^{3+} is first reduced to Au^{1+} and then to Au^0; moreover, the conversion mechanism between the different valence states is considered reversible. The conversion kinetics behavior of the AuNP valence states is illustrated in Figure S4. The Au^{3+} valence state oscillation reveals a reversible process. Specifically, there is a reversible conversion between the valence states Au^{1+} and Au^{3+} (Au^{3+} $\overset{k_1}{\underset{k_{-1}}{\rightleftharpoons}}$ Au^{1+}) and Au^{1+} and Au^0 (Au^{1+} $\overset{k_2}{\underset{k_{-2}}{\rightleftharpoons}}$ Au^0) during the ion bombardment process. Therefore, since the atomic concentration of Au^0 and Au^{1+} increases and decreases, respectively, we infer that the rate constants k_1 and k_{-1} are quantitatively comparable to each other, while k_2 is much larger than k_{-2}. This implies a kinetic conversion mechanism between the valence states from Au^{3+} to Au^{1+} and then Au^{1+} to Au^0, and there is no direct transition from Au^{3+} to Au^0.

The valence-band near the Fermi level of AuNPs can be studied using the Au 5d XPS spectra.[32] Typical spectra for AuNPs with different Ar$^+$ ion bombardment times are shown in Figure S5. The structure observed between 1 and 10 eV below the Fermi level arises from the relative energy of the ion remaining after electron emission from the Au 5d state.[33] The experimental result shows that the peak shift toward lower energy, this is most evident in the two-dimensional contour map of the Au 5d spectra, as shown in Figure 6. The dotted line shows the time evolution of the binding energies of the
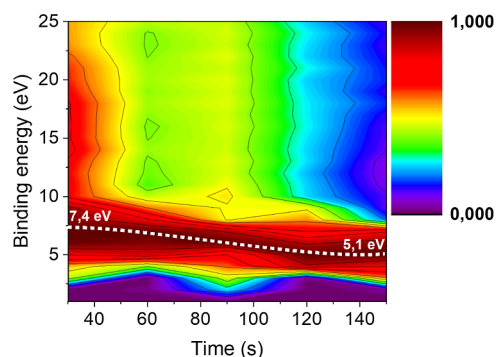
Figure 6. Two-dimensional contour map of the Au 5d spectra. The 2D plot was performed with all data recorded after each sputter etching.

valence-band electrons. The data show a clear decrease in the binding energy from ~7.4 to ~5.1 eV as the sputtering exposure time increases. It should be noted that the Fermi level and the density of states in the valence band show a strong dependence on the NP size.[34] Therefore, the observed results are related to the changes in valence states due to the desorbing O(Cl)-containing species and the decrease in the NP size after each sputter etching. This can be interpreted as a reduction in the band gap related to the conversion of Au^{3+} and Au^{1+} to Au^0 valence states and the decrease in the size of the AuNPs.

■ CONCLUSIONS

AuNPs with different Au oxidation valence states (Au^{3+}, Au^{1+}, and Au^0) have been successfully obtained by solid-state thermal dewetting of gold thin films. It was possible to fine-tune the concentration of valence states by means of Ar$^+$ ion bombardment using the ion-induced reduction effect. The stability of gold complexes was related to the electronegativity of the donor atom bonded directly to the Au, that is, the

stability increases when the donor atom is less electronegative.[35] The results obtained show a tuning effect on the valence states of Au using low-energy Ar$^+$ ion bombardment as a function of time. We emphasize that the physicochemical properties of the compounds depend on the particle size[36] and valence states.[37] Besides, the valence band is modified, showing a decrease in the binding energy from ~7.4 to ~5 eV as the sputtering exposure time increases. Thus, valence state tuning in AuNPs brings attractive physical and chemical properties and extend its potential material science applications.

EXPERIMENTAL SECTION

Materials. The Au used in this work was a gold wire of 99.99% purity and diameter of 1 mm, acquired from Kurt J. Lesker. NaCl substrates (sodium chloride single crystal) with orientation (100) and size of 10 × 10 × 10 mm were purchased from US Research Nanomaterials. Ultrapure water (18.25 MΩ cm) was used in the suspension of AuNPs.

Synthesis of AuNPs by the Dewetting Process. The synthesis method used here is based on forming AuNPs through the dewetting process. In this method, an Au thin film of 40 nm was deposited by evaporation on NaCl substrates. The evaporation was carried out in a vacuum chamber (EDWARDS BOC/AUTO 306 Thermal Evaporator) with a rate of 1 mm/s at ~3 × 10^{-3} Pa. Then, the substrates were removed from the vacuum chamber and exposed to thermal treatment at a temperature of 600 °C for 30 min. During this time, the Au thin film goes through a process in which the film on the substrate ruptures into an ensemble of separated nanoparticles (dewetting). Finally, after thermal treatment, the nanoparticles are collected by dripping the water on the surface of the substrate.

Characterization Techniques. Images of AuNPs synthesized were obtained by SEM using a Tescan GAIA3 FIB-SEM system, with which it is also possible to obtain compositional information of the AuNPs by energy EDS. The particle size distributions were determined using image analysis of SEM images. Absorption spectra (from 400 to 800 nm) of AuNPs suspended were obtained using Thermo Scientific's 10S UV−vis spectrophotometer equipment. The chemical states of the AuNPs were investigated by XPS using a Thermo Alpha 110 hemispherical analyzer. The XPS measurement was performed using an Al cathode (h = 1486.6 eV) as the X-ray source in the CPM using 40 eV pass energy.

ASSOCIATED CONTENT

Supporting Information

The Supporting Information is available free of charge at https://pubs.acs.org/doi/10.1021/acsomega.2c04259.

Complementary results of the temporal evolution of AuNP composition and conversion kinetics of AuNP valence states (PDF)

AUTHOR INFORMATION

Corresponding Author

Alba Avila − Centro de Microelectrónica (CMUA), Departamento de Ingeniería Eléctrica y Electrónica, Universidad de los Andes, Bogotá 111711, Colombia; orcid.org/0000-0003-1241-2080; Email: a-avila@uniandes.edu.co

Authors

Gustavo Lanza − Centro de Microelectrónica (CMUA), Departamento de Ingeniería Eléctrica y Electrónica, Universidad de los Andes, Bogotá 111711, Colombia; orcid.org/0000-0003-4059-1493

Mawin J. Martinez Jimenez − Centro de Microelectrónica (CMUA), Departamento de Ingeniería Eléctrica y Electrónica, Universidad de los Andes, Bogotá 111711, Colombia; orcid.org/0000-0001-5666-6416

Fernando Alvarez − Instituto de Física Gleb Wataghin (IFGW), Universidade Estadual de Campinas, Sao Paulo 13083-970, Brazil; orcid.org/0000-0002-9393-1298

Jaime Andres Perez-Taborda − Sociedad Colombiana de Ingeniería Física (SCIF), Valledupar 111711, Colombia; Grupo de Nanoestructuras y Física Aplicada (NANOUPAR), Universidad Nacional de Colombia Sede De La Paz, La Paz 202010, Colombia; orcid.org/0000-0002-5202-9708

Complete contact information is available at:
https://pubs.acs.org/10.1021/acsomega.2c04259

ACKNOWLEDGMENTS

REFERENCES

(1) Huang, X.; El-Sayed, M. A. Gold nanoparticles: Optical properties and implementations in cancer diagnosis and photothermal therapy. *J. Adv. Res.* **2010**, 1, 13−28.

(2) Asadi, S.; Bianchi, L.; De Landro, M.; Korganbayev, S.; Schena, E.; Saccomandi, P. Laser-induced optothermal response of gold nanoparticles: From a physical viewpoint to cancer treatment application. *J. Biophotonics* **2021**, 14, No. e202000161.

(3) Ielo, I.; Rando, G.; Giacobello, F.; Sfameni, S.; Castellano, A.; Galletta, M.; Drommi, D.; Rosace, G.; Plutino, M. R. Synthesis, chemical−physical characterization, and biomedical applications of functional gold nanoparticles: A review. *Molecules* **2021**, 26, 5823.

(4) Mie, G. Beiträge zur Optik trüber Medien, speziell kolloidaler Metallösungen. *Ann. Phys.* **1908**, 330, 377−445.

(5) Si, P.; Razmi, N.; Nur, O.; Solanki, S.; Pandey, C. M.; Gupta, R. K.; Malhotra, B. D.; Willander, M.; de la Zerda, A. Gold nanomaterials for optical biosensing and bioimaging. *Nanoscale Adv.* **2021**, 3, 2679−2698.

(6) Bär, J.; de Barros, A.; de Camargo, D. H.; Pereira, M. P.; Merces, L.; Shimizu, F. M.; Sigoli, F. A.; Bufon, C. C. B.; Mazali, I. O. Silicon microchannel-driven Raman scattering enhancement to improve gold nanorod functions as a SERS substrate toward single-molecule detection. *ACS Appl. Mater. Interfaces* **2021**, 13, 36482−36491.

(7) Hammami, I.; Alabdallah, N. M.; jomaa, A.; kamoun, M. Gold nanoparticles: Synthesis properties and applications. *J. King Saud Univ., Sci.* **2021**, *33*, 101560.

(8) Clarke, C.; Liu, D.; Wang, F.; Liu, Y.; Chen, C.; Ton-That, C.; Xu, X.; Jin, D. Large-scale dewetting assembly of gold nanoparticles for plasmonic enhanced upconversion nanoparticles. *Nanoscale* **2018**, *10*, 6270−6276.

(9) Müller, C. M.; Spolenak, R. Microstructure evolution during dewetting in thin Au films. *Acta Mater.* **2010**, *58*, 6035−6045.

(10) Sankar, M.; He, Q.; Engel, R. V.; Sainna, M. A.; Logsdail, A. J.; Roldan, A.; Willock, D. J.; Agarwal, N.; Kiely, C. J.; Hutchings, G. J. Role of the support in gold-containing nanoparticles as heterogeneous catalysts. *Chem. Rev.* **2020**, *120*, 3890−3938.

(11) Narayan, N.; Meiyazhagan, A.; Vajtai, R. Metal nanoparticles as green catalysts. *Materials* **2019**, *12*, 3602.

(12) Casaletto, M.; Longo, A.; Martorana, A.; Prestianni, A.; Venezia, A. XPS study of supported gold catalysts: the role of Au0 and Au+ δ species as active sites. *Surf. Interface Anal.* **2006**, *38*, 215−218.

(13) Zheng, J.; Lyu, Y.; Qiao, M.; Veder, J. P.; Marco, R. D.; Bradley, J.; Wang, R.; Li, Y.; Huang, A.; Jiang, S. P.; et al. Tuning the Electron Localization of Gold Enables the Control of Nitrogen-to-Ammonia Fixation. *Angew. Chem., Int. Ed.* **2019**, *58*, 18604−18609.

(14) Pakrieva, E.; Kolobova, E.; Kotolevich, Y.; Pascual, L.; Carabineiro, S. A.; Kharlanov, A. N.; Pichugina, D.; Nikitina, N.; German, D.; Zepeda Partida, T. A.; et al. Effect of gold electronic state on the catalytic performance of nano gold catalysts in n-octanol oxidation. *Nanomaterials* **2020**, *10*, 880.

(15) Miller, K. K.; Shancita, I.; Bhattacharia, S. K.; Pantoya, M. L. Surface modifications of plasma treated aluminum particles and direct evidence for altered reactivity. *Mater. Des.* **2021**, *210*, 110119.

(16) Di, L.; Zhang, J.; Zhang, X.; Wang, H.; Li, H.; Li, Y.; Bu, D. Cold plasma treatment of catalytic materials: a review. *J. Phys. D: Appl. Phys.* **2021**, *54*, 333001.

(17) Morales, M.; Merlo, R.; Droppa, R.; Alvarez, F. Self-organized 2D Ni particles deposited on titanium oxynitride-coated Si sculpted by a low energy ion beam. *J. Phys. D: Appl. Phys.* **2014**, *47*, 195303.

(18) Pabón, B. M.; Beltrán, J. I.; Sánchez-Santolino, G.; Palacio, I.; López-Sánchez, J.; Rubio-Zuazo, J.; Rojo, J.; Ferrer, P.; Mascaraque, A.; Muñoz, M. C.; et al. Formation of titanium monoxide (001) single-crystalline thin film induced by ion bombardment of titanium dioxide (110). *Nat. Commun.* **2015**, *6*, 6147.

(19) Blimes, S.; Mandelbaum, P.; Alvarez, F.; Victoria, N. Surface and electronic structures of titanium dioxide photocatalyst. *J. Phys. Chem. B* **2000**, *104*, 9851−9858.

(20) Xie, F.; Gong, L.; Liu, X.; Tao, Y.; Zhang, W.; Chen, S.; Meng, H.; Chen, J. XPS studies on surface reduction of tungsten oxide nanowire film by Ar+ bombardment. *J. Electron Spectrosc. Relat. Phenom.* **2012**, *185*, 112−118.

(21) Klimmer, A.; Ziemann, P.; Biskupek, J.; Kaiser, U.; Flesch, M. Size-dependent effect of ion bombardment on Au nanoparticles on top of various substrates: thermodynamically dominated capillary forces versus sputtering. *Phys. Rev. B: Condens. Matter Mater. Phys.* **2009**, *79*, 155427.

(22) Datta, D.; Chettah, A.; Maiti, A.; Satpati, B.; Sahoo, P. Ultraviolet and Infrared luminescent Au-rich nanostructure growth in SiO2 by burrowing and inverse Oswald ripening process. *Sci. Rep.* **2019**, *9*, 14978.

(23) Avila, A.; Lanza, G.; Perez-Taborda, J. Método de Síntesis Fisica de Nanopartículas Métalicas. *Superintendencia de Industria y Comercio NC2021/000297*, 2022.

(24) Amendola, V.; Pilot, R.; Frasconi, M.; Maragò, O. M.; Iatì, M. A. Surface plasmon resonance in gold nanoparticles: a review. *J. Phys.: Condens. Matter* **2017**, *29*, 203002.

(25) Zimbone, M.; Baeri, P.; Calcagno, L.; Musumeci, P.; Contino, A.; Barcellona, M. L.; Bonaventura, G. Dynamic light scattering on bioconjugated laser generated gold nanoparticles. *PLoS One* **2014**, *9*, No. e89048.

(26) Hammer, P.; Victoria, N.; Alvarez, F. Electronic structure of hydrogenated carbon nitride films. *J. Vac. Sci. Technol., A* **1998**, *16*, 2941−2949.

(27) Sylvestre, J.-P.; Poulin, S.; Kabashin, A. V.; Sacher, E.; Meunier, M.; Luong, J. H. Surface chemistry of gold nanoparticles produced by laser ablation in aqueous media. *J. Phys. Chem. B* **2004**, *108*, 16864−16869.

(28) Dwivedi, N.; Yeo, R. J.; Tan, H. R.; Stangl, R.; Aberle, A. G.; Bhatia, C. S.; Danner, A.; Liao, B. Evidence for chemicals intermingling at Silicon/Titanium oxide (TiOx) interface and existence of multiple bonding states in monolithic TiOx. *Adv. Funct. Mater.* **2018**, *28*, 1707018.

(29) Kim, S. M.; Kim, K. K.; Jo, Y. W.; Park, M. H.; Chae, S. J.; Duong, D. L.; Yang, C. W.; Kong, J.; Lee, Y. H. Role of anions in the AuCl3-doping of carbon nanotubes. *ACS Nano* **2011**, *5*, 1236−1242.

(30) He, D.; Wang, B.; Wu, T.; Su, H.; Zhang, X.; Ren, Y.; Xu, G.-L.; Liu, Z.; Wang, J.; Amine, K.; et al. TiO2 Nanocrystal-Framed Li2TiSiO5 Platelets for Low-Voltage Lithium Battery Anode. *Adv. Funct. Mater.* **2020**, *30*, 2001909.

(31) Fong, Y.-Y.; Visser, B. R.; Gascooke, J. R.; Cowie, B. C.; Thomsen, L.; Metha, G. F.; Buntine, M. A.; Harris, H. H. Photoreduction kinetics of sodium tetrachloroaurate under synchrotron soft X-ray exposure. *Langmuir* **2011**, *27*, 8099−8104.

(32) Liu, H.; Mun, B. S.; Thornton, G.; Isaacs, S. R.; Shon, Y.-S.; Ogletree, D. F.; Salmeron, M. Electronic structure of ensembles of gold nanoparticles: Size and proximity effects. *Phys. Rev. B: Condens. Matter Mater. Phys.* **2005**, *72*, 155430.

(33) Fadley, C.; Shirley, D. Electronic densities of states from X-ray photoelectron spectroscopy. *J. Res. Natl. Bur. Stand., Sect. A* **1970**, *74*, 543.

(34) Zhang, Y.; Pluchery, O.; Caillard, L.; Lamic-Humblot, A.-F.; Casale, S.; Chabal, Y. J.; Salmeron, M. Sensing the charge state of single gold nanoparticles via work function measurements. *Nano Lett.* **2015**, *15*, 51−55.

(35) Đurović, M. D.; Bugarčić, Ž. D.; van Eldik, R. Stability and reactivity of gold compounds−From fundamental aspects to applications. *Coord. Chem. Rev.* **2017**, *338*, 186−206.

(36) Ishida, T.; Murayama, T.; Taketoshi, A.; Haruta, M. Importance of size and contact structure of gold nanoparticles for the genesis of unique catalytic processes. *Chem. Rev.* **2019**, *120*, 464−525.

(37) De Anda Villa, M.; Gaudin, J.; Amans, D.; Boudjada, F.; Bozek, J.; Evaristo Grisenti, R.; Lamour, E.; Laurens, G.; Macé, S.; Nicolas, C.; et al. Assessing the surface oxidation state of free-standing gold nanoparticles produced by laser ablation. *Langmuir* **2019**, *35*, 11859−11871.